

# Study of a Hybrid Actuated Exoskeleton for Upper Limb Rehabilitation

Dimitar Chakarov<sup>a</sup>, Ivanka Veneva<sup>b</sup>, Mihail Tsveov<sup>c</sup> and Pavel Venev<sup>d</sup>

*Institute of Mechanics, BAS, "Acad. G. Bonchev" Str., Block 4, Sofia 1113, Bulgaria*

**Keywords:** Exoskeleton, Transparency, Safety, Pneumatic, Electric, Hybrid, Actuation, Human, Therapeutic, Dynamic Simulations, Mechanical Impedance, Resistive Torque.

**Abstract:** In this paper, an upper arm rehabilitation exoskeleton is studied. An appropriate solution is sought for the exoskeleton design and actuation that provides transparency and natural safety as well as sufficient force and performance. To achieve this, a hybrid actuation with back-drivable electric and pneumatic drives is studied. A hybrid actuation controller is introduced, in which pneumatic drive takes care of the initial force response, and the electric drive complements the pneumatic drive. In the paper, the feasibility of the basic therapy modes "patient in charge" and "robot in charge" is simulated. An approach for dynamic estimation of elastic propulsion in the second joint through imposed motions is used. The influences of the inertial, frictional, gravitational, and elastic forces that resulted from the hand and the exoskeleton impedance are reported. The pneumatic drive's influence as an elastic balance of the gravitational forces is considered. Finally, a conclusion and discussion are added.

## 1 INTRODUCTION

Rehabilitation robots have been used in the initial stages of rehabilitation when the patient is unable to move his limbs independently. Unlike robots that are designed to assist completely paralyzed patients, rehabilitative exoskeletons must be able to respond to any movement (even minimal ones) that the patient performs (Jarrasse, 2014).

After the patient has regained some degree of mobility, mutual movement control should be possible (Hogan, 2006). Therefore, one of the main characteristics that exoskeletons must possess is transparency. The exoskeleton has to be fully tolerant (without influence) to the patient's movement if he can do it alone.

The forces which restrict the movement are a result of mechanical impedance of the exoskeleton, including the inertia, friction, and stiffness. Gravitational forces must be added to these forces as well.

There are two main approaches to reducing the impedance of a device: the active and the passive approaches. The more common way is to use active control. This approach is usually implemented as a feedforward or feedback control (Bergamasco, 1994).

Two control algorithms for rehabilitation exoskeletons are currently used: impedance and admittance (Carignan, 2000). Impedance one senses the human motion and controls the device's force. Admittance one senses the human force and controls the device's motion.

The active approach is used widely for impedance reduction but without good safety and transparency cause of sensor's noise or resolution; calculation time; servo instability. The passive approach, missing the servo delay, gives safety and transparency.

To adjust the passive impedance, passive or natural compliant elements are usually used, like the widely known "serial elastic actuation" (SEA), where the impedance is limited to the stiffness values of serial attached torsion spring (Veneman, 2006). The elastic elements can also be attached in parallel to the

<sup>a</sup> <https://orcid.org/0000-0002-2312-5725>

<sup>b</sup> <https://orcid.org/0000-0001-5501-7668>

<sup>c</sup> <https://orcid.org/0000-0001-5051-4411>

<sup>d</sup> <https://orcid.org/0000-0001-7809-3540>

actuator, known as "parallel elastic actuation" (PEA). Thus, also a beneficial effect on natural dynamics can be obtained (Verstraten, 2016).

For natural compliance implementation, pneumatic artificial muscles (PAMs) are widely used (Daerden, 2002), (Caldwell, 2007). They have good power over weight (volume) ratios for lightweight systems. The impedance is low over a wide frequency range because of the low inertia and gas compliance. The problem is that performance is decreased by a bad dynamic force response and bad positioning.

The disadvantages can be lowered by improving the muscle structure. Some studies are based on a hybrid actuation control strategy. One approach uses PAMs pair and a low-inertial DC motor in parallel (Sardellitti, 2007). The muscles do the low-frequency macro torque, and the DC motor compensates for the torque error. Another approach is known (Noda, 2014), where the authors propose the use of a Bowden cables to transmit the power generated by PAM's to the exoskeleton joints, and small electric motors are installed in the joints to compensate for the uncertainty generated by PAM's and Bowden cables. In another hybrid approach, a pair of air muscles are combined with DC-harmonic drive (Aguilar-Sierra, 2015). There, PAMs ensure the magnitude of the torque, and the DC gives the precision. Another solution combined PAM with a magnetic brake for enhanced security (Shin, 2014).

The aim of this work is to study and evaluate an upper limb exoskeleton with appropriate design and actuation to achieve transparency and natural safety on the one hand and force impact and performance on the other hand in the process of upper-arm rehabilitation.

The article is constructed as follows: At first, the article revealed the mechanical structure and actuation of a light arm exoskeleton with hybrid actuation. Second, the authors built a hybrid actuation control algorithm suitable for a wide range of therapeutic procedures. Third, the authors made dynamic simulations to estimate the joint torques for two therapeutic modes: "patient in charge" and "robot in charge". In the end, there is a discussion and conclusion.

## 2 MECHANICAL STRUCTURE AND ACTUATION OF AN UPPER LIMB EXOSKELETON

One way to design a rehabilitation exoskeleton is to use a passive approach. This means having extremely

light attachments to the limbs and putting all heavy components on the torso or the ground. The exoskeleton arm prototype is constructed of aluminum segments (Figure: 1) with variable lengths for fast and easy adjusting for different user sizes. Attaching the human arm to segments is done through soft shells with bands. The exoskeleton arm includes four segments 1, 2, 3, 4 connected by 4 rotating joints J1, J2, J3 and J4 with a total of 4 d.o.f., two over the shoulder and two over the elbow. The masses of the four segments are  $M1=0.318$  kg,  $M2=0.367$  kg,  $M3=0.321$  kg and  $M4=0.194$  kg.

The initial arm and forearm lengths are  $L1=0.286$  m and  $L2=0.370$  m. The ranges of the joints J1, J2, J3 and J4 are  $110^\circ$ ,  $110^\circ$ ,  $150^\circ$  and  $135^\circ$ . The exoskeleton is designed according to the requirements of the "activities of daily living" (ADL), as they are rated by (Perry, 2007) and (Abane, 2016).

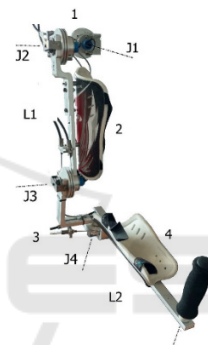


Figure 1: Picture of exoskeleton arm prototype.

To build a drive system for one powerful exoskeleton, the actuators must be big and heavy. Small, light motors with high gear ratios can also give enough force, but gears reduce dynamic performance, so feedback control techniques must be used (Ermolov, 2016). In the case of an exoskeleton for rehabilitation, it is assumed that the actuators should be back drivable, and the exoskeleton should have low friction and negligible backlash (Garrec, 2008).

To meet these requirements, a pneumatic drive based on PAMs is used. It provides natural compliance and safety. It also makes it possible to adjust the compliance according to the rehabilitation control strategies. To overcome the limitations of air muscles and to achieve the full range of therapeutic interventions, we develop a hybrid type, with pneumatic and electric drives in parallel.

The joint pneumatics include braided PAMs with diameter  $D = 0.016$  m and initial length  $L_n=0.390$  m. The maximum contraction achieved is  $C_{max}=0.156$  m. Bundles of several muscles, like in (Chakarov, 2017), are used to easily modify the power and compliance.

All the muscles of a single PAM actuator are connected at both ends and fed in parallel through a single valve. Another valve is used for discharging.

A picture of the actuation prototype with parallel pneumatic and electric drives is shown in Figure: 2. In the fixed base 0, there are two wheels 1 and 2 connected to a timing belt. This achieves a gear ratio of 2: 1. A back drivable DC-motor, coupled with a low reduction gear, is connected to wheel 1. An additional washer adapted for winding a cable is attached to wheel 2. Cable transmissions (Bowden cables)  $T_1$  and  $T_2$  are used for the coupling between pulley two and similar pulley mounted in the joint of the exoskeleton arm. The pneumatic drive consists of two PAM actuators, "a" and "b" attached at one end to the fixed base 0 and at the other end to both sides of the timing belt, as shown in Figure 2. In this way, PAM actuators work in an antagonistic circuit, creating a torque of wheel 2. Pressure sensors are mounted on each supply pipeline. A high precision rotation sensor is mounted in the exoskeleton joint to measure the angular displacement.

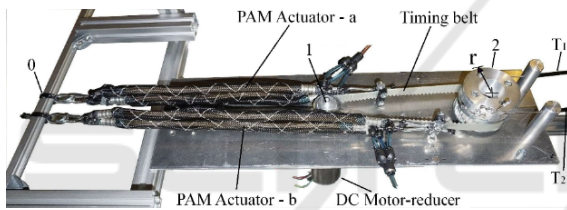


Figure 2: Joint actuation with parallel pneumatic and electric drives - picture of the actuation prototype.

The braided PAM behaves as a spring with variable compliance. A simplified static model is made used in (Caldwell, 2007) and (Chou, 1996) simulating a nonlinear quadratic spring. This model is modified for several muscles in a bundle (Chakarov, 2017). The forces of the bundles "a" and "b" are presented with equalities:

$$P_a = (k_{a0} + k_{a1} p_a) (L_n - r(q - q^{\max})) (C_{\max} - r(q - q^{\max})) \quad (1)$$

$$P_b = (k_{b0} + k_{b1} p_b) (C_{\max} - r(q - q^{\min})) (L_n - r(q - q^{\min})) \quad (2)$$

where  $k_{a0}$ ,  $k_{b0}$ ,  $k_{a1}$ , and  $k_{b1}$  are empirically discovered coefficients depending on the muscles count  $m_a$  and  $m_b$  in the bundle;  $p_a$  and  $p_b$  are the supply pressures of the bundles;  $q$  is the joint angle and  $r$  is the pulley radius. The antagonistic action of the PAM actuators in each joint creates pneumatically generated torque:

$$Q_p = (P_b - P_a) r \quad (3)$$

In the design that is considered, the two PAM bundles "a" and "b" are mounted and include 2 and 4

muscles, respectively, the coefficients have the following values:  $k_{a0} = 603$ ,  $k_{a1} = 8.61$ ,  $k_{b0} = 1245$ , and  $k_{b1} = 17.43$ .

A back drivable DC-motor coupled with a low reduction gear is connected to wheel 1 for the parallel action with the PAM actuators (Figure 2). A low-inertia Maxon motor EC-i 52 and a NE Nema Series planetary gearhead with a gear ratio of 10:1 are used. Since a belt transmission with a gear ratio of 2:1 is used in the structure, the overall gear ratio of the transmission from the electric motor to the wheel 2 is  $n = 20:1$ . The parameters of the motor and gearbox are listed in Table. 1.

Table 1: Motor and gear parameters.

Motor nominal power		180	W
Motor nominal voltage		24	V
Motor nominal torque		434	mNm
Max. motor efficiency	$\eta_m$	90	%
Motor rotor inertia	$J_m$	$170 \cdot 10^{-7}$	kgm <sup>2</sup>
Gearhead reduction		10 : 1	
Gearhead efficiency	$\eta$	89	%
Gearhead inertia	$J_r$	$5.1 \cdot 10^{-7}$	kgm <sup>2</sup>
Gearhead max. accel. output torque		7	Nm
Belt transmission reduction		2:1	
Transmission's Coulumb friction	$T_c$	0.360	Nm
Transmission's viscous friction	$N$	0.250	Nm.s/rad
Radius of pulley 2	$r$	0.0315	m

### 3 REHABILITATION EXOSKELETON CONTROL

The rehabilitation exoskeleton must provide enough force to assist or resist the motor activity of the patient or to follow human movements with no resistance (Jarrasse, 2014). In general, the control of a rehabilitation exoskeleton can be divided into two ideal modes that cover the full range of therapeutic tasks: "robot in charge" and "patient in charge" (Veneman, 2006). In the "patient-in-charge", the interactive forces between the exoskeleton and patient must be close to zero (low perceived robot impedance). Ideally, if the interactive forces between the robot and the patient are zero, it means the robot is completely transparent. In the "robot-in-charge", the robot must have enough bandwidth and power to achieve the desired position with high impedance. To

meet these requirements, an exoskeleton with the described design is developed, including hybrid electric and pneumatic drives.

The natural pneumatic drive's impedance takes care of the initial response in order to provide security and transparency. The active impedance of the hybrid actuation creates a subsequent response that is generated by the force feedback and feed-forward compensations.

The joint level impedance controller is selected as shown in the block diagram of Figure: 3. As the reference for the impedance controller, a trajectory and an impedance value are selected. The joint position  $\Delta q_d$  and joint stiffness  $K_d$  represent the references in the impedance controller. Feedforward compensations are also included in the block diagram. The joint force command (Fig. 3) is represented by equality:

$$Q = Q_d + Q_f - Q_h \quad (4)$$

where  $Q_d$  denotes the desired torque in the joint space, calculated according to the desired joint stiffness  $K_d$  and the difference between the desired and measured joint position ( $\Delta q_d - \Delta q$ );  $Q_f$  denotes the joint force command according to the impedance feedforward model;  $Q_h$  denotes the torque of the forces applied by the patient on the exoskeleton segments.

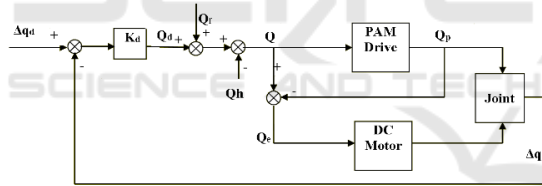


Figure 3: Impedance controller of the hybrid actuated joint.

By monitoring the pressures  $p_a$  and  $p_b$  of the two PAM actuators and the joint angle  $q$  according to equations (1), (2) and (3), the pneumatic drive torque  $Q_p$  can be monitored. The difference between the joint torque command  $Q$  and the real pneumatic drive torque  $Q_p$ , determines the torque tracking error  $Q_e$  that is a force command for the electric motor:

$$Q_e = Q - Q_p \quad (5)$$

An open loop DC motor current controller is used to achieve the desired joint torque and to compensate for the slow dynamics of the pneumatic drive.

## 4 SIMULATION AND PERFORMANCE EVALUATION

To assess the feasibility of the two main therapeutic modes, "robot in charge" and "patient in charge" using the "hybrid actuation approach", dynamic simulations of a driven joint are conducted. The dynamics of parallel elastic actuation are evaluated using cyclic motion (Verstraten, 2016). The simulations were performed using harmonic motions with an amplitude  $q_m$  that is imposed on the second joint J2 of the arm. The law of motion of the position, velocity, and acceleration is:

$$q = q_{\max} \sin(\omega t) + q_0 \quad (6)$$

$$\dot{q} = q_{\max} \omega \cos(\omega t) \quad (7)$$

$$\ddot{q} = -q_{\max} \omega^2 \sin(\omega t) = -\omega^2 (q - q_0) \quad (8)$$

where  $\omega$  is the periodic motion frequency, and  $q_0$  is the starting position of the arm (Figure: 4). An uniform frequency variation was chosen in the range of  $\omega = [1, \dots, 6]$  rad/s for time  $t = [1, \dots, 6]$  s. The joint angle  $q$  determines the position of the hand. Considering that the zero angle is the Y axis, we conduct the simulations in the angular range of  $[180^\circ - 290^\circ]$  with the primary angle  $q_0 = 235^\circ$  and amplitude  $q_m = 55^\circ$  being the limits of the range of motion.

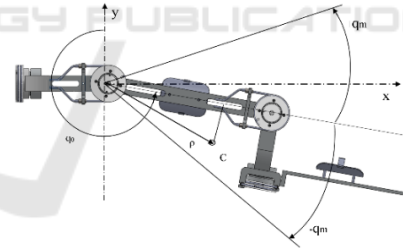


Figure 4: Exoskeleton arm performing harmonic motion with amplitude  $q_m$  from starting position  $q_0$ .

The resistance torque in the joint, as a result of motor inertia, exoskeleton inertia, friction, and gravity is as follows:

$$Q_r = Q_J^m + Q_J^l + Q_{fr} + Q_g \quad (9)$$

In the above equations, the torque of gravity  $Q_g$  of the exoskeleton with the mass  $M_1$  and the radius  $\rho = [\rho_1; \rho_2]^T$  of the mass center C is as follows:

$$Q_g = M_1 g [-\rho_1 \sin q + \rho_2 \cos q] \quad (10)$$

where  $g$  is the gravity acceleration coefficient.

The viscous and Coulomb friction torques in the joint as a result of the friction in the PAM actuators and in the Bowden cables are as follows:

$$Q_{fr} = N\dot{q} + T_c \text{sign}(\dot{q}) \quad (11)$$

where  $N$  is the viscous friction coefficient, and  $T_c$  is the Coulomb friction torque. These coefficients are generalized measures of the different energy effects in the PAM actuators, Bowden cables, bearings, and other components for which empirical rather than analytical estimates are known (Chou, 1996), (Schiele, 2006).

The inertial members in equation (9) are represented by the following equations:

$$Q_J^m = (J_m + J_{tr}) \frac{n^2}{C} \ddot{q} \quad (12)$$

$$Q_J^l = J_l \ddot{q} \quad (13)$$

which express the torques of motor inertia  $Q_J^m$  and load inertia  $Q_J^l$ . Here,  $J_m$ ,  $J_{tr}$  and  $J_l$  are the inertias of the rotor, of the transmission and of the load, respectively; and  $n$  is the gear ratio.  $C$  is gear head efficiency function, which, according to (Giberti, 2010), gives the effects of the power flow reversal as follows:

- $C = 1/\eta_{tr}$  - the motor drives the load; and
- $C = \eta_{tr}$  - the motor is driven by the load.

The simulations were sequentially conducted for the two main therapeutic modes: “patient in charge” and “robot in charge”.

#### 4.1 The “Patient in Charge” Mode

In this mode, the authors suggest that the patient has the motor capacity to move his hand independently. In passive mode, the electric and pneumatic drives do not generate active forces. The torque of the forces that are exerted by the human  $Q_h$  on the exoskeleton to overcome the exoskeleton mechanical impedance is determined of the resistance torque (9) involves inertial, frictional and gravitational forces as well as elastic forces according to the equation:

$$Q_h = Q_J^m + Q_J^l + Q_{fr} + Q_g - Q_p \quad (14)$$

Above the torque  $Q_p$  is determined by the elastic forces of the PAM actuators which are fed by the given pressures  $p_a$  and  $p_b$  according to (1), (2) and (3). In the current simulations,  $Q_p$  represents the torque as a result of the passive stiffness of the pneumatic drive.

It is accepted that the mass and inertia of the load are equal to those of the exoskeleton, which means that  $M_l = M_e$  and  $J_l = J_e$ , respectively. The total mass of the exoskeleton’s moving parts 2,3 and 4 are  $M_e = 0.882$  kg, and the coordinates of the mass center  $C$  are  $\rho = [0.219; 0.039]^T$  (Figure: 4). The inertia of the exoskeleton arm to the axis of joint J2 is  $J_e = 0.061$  kgm<sup>2</sup>. The values of the remaining mechanical parameters from (11) and (12) are shown in Table 1. The gearbox efficiency function is  $C = \eta$ , (the motor is driven by the patient). The described patient-initiated harmonic motion in equations (6), (7), and (8) is examined using an increasing frequency. Adopted is an amplitude of movements of  $q_m = 55^\circ$  from the initial position  $q_0 = 235^\circ$ .

The change of the torque of motor inertia (12) and the torque of load inertia (13), as well as the torques of viscous and Coulomb friction (11), are shown in Figure: 5. These torques are independent of the arm position but depend on the oscillation frequency. The graph also shows the change in the torque of gravity (10) that depends mainly on the position of the arm. Figure: 5 (a) and (b) shows the effect of the gear ratio for  $n = 90$  and  $n = 20$  respectively. Increasing the gear ratio significantly increases the influence of the torque of motor inertia. Then, at “patient in charge”, the faster patient initiated motions are associated with higher interaction forces. In the studied exoskeleton, a gear ratio  $n = 20$  was chosen, and the resistance torques are shown in Figure:5(b).

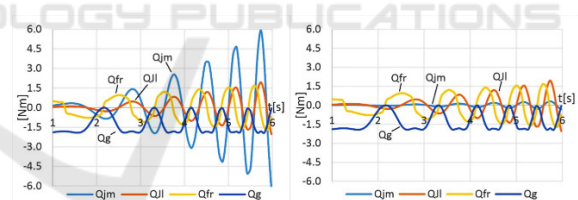


Figure 5: Resistance joint torques according to (9), which are generated by the patient’s harmonic motion with a uniform increase in the frequency and ratio of the joint gear: a)  $n = 90$  and b)  $n = 20$ .

Fluctuation in the total joint resistance (9) is shown in the graph in Figure: 6. At low frequencies, it is mainly a result of gravitational loads, and at high frequencies, it results mainly from inertial loads.

The graph of Figure: 6 also shows the passive torque of the pneumatic drive  $Q_p$ . It is calculated according to (1), (2), and (3), where  $q_0 + q_m$  determines the maximum position  $q^{\max}$  for one PAM actuator and the minimum position  $q^{\min}$  for the other, respectively  $q_0 - q_m$  determines  $q^{\min}$  and  $q^{\max}$ . In this workspace position ( $q_0 = 235^\circ$ ), the pressure of the two PAM actuators is selected, respectively  $p^a = 10$  kPa and  $p^b$

= 0. The pneumatic drive acts as an elastic balancer of the gravity load. The torque of the elastic forces of the PAM actuators oscillates with the oscillations of the position, but its average is constant. The resistance torque is mainly compensated by the torque of the elastic forces. In another position of the workspace, such compensation can be achieved by other pressures of the PAM actuators.

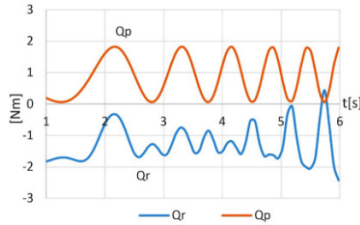


Figure 6: Torque of total joint resistance  $Q_r$  and torque of pneumatic drive  $Q_p$ .

The total torque calculated according to equation (14) is shown in Figure: 7. It represents the torque of the interaction forces that are applied to the hand of the patient initiating the movement. The simulation shows that this torque does not exceed 1.6 Nm.

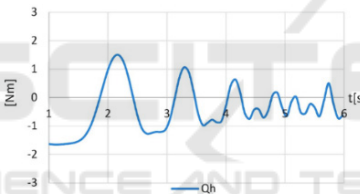


Figure 7: Torque of the interaction forces that are applied to the hand of the patient initiating the movement.

In active mode, according to the control scheme of Figure: 3, the resistance torque in the joint (9) as a result of exoskeleton mechanical impedance is considered to be a reference for the feedforward compensations  $Q_f = Q_r$ . In order to obtain complete transparency for the patient  $Q_h=0$ , assuming that  $Q_d = 0$ , the joint force command (4) will have the form  $Q = Q_r$ . This command is assigned for the implementation of the hybrid pneumatic and electric drive.

#### 4.2 The “Robot in Charge” Mode

In this mode, the authors suggest that the patient does not resist  $Q_h=0$  (fully immobilized patient). This is an active mode in which the joint force command is determined according to the hybrid control scheme of Figure: 3. The resistance torque in the joint (9) determined by the patient’s and the exoskeleton’s impedance as inertial, friction and gravitational forces

is considered to be a reference for the feedforward compensations  $Q_f = Q_r$ . Assuming that  $Q_d = 0$ , according to (4) and (5), the joint force command to the electric drive will be as follows

$$Q_e = Q_J^m + Q_J^l + Q_{fr} + Q_g - Q_p \quad (15)$$

The joint actuators drive the exoskeleton arm and the patient’s hand. The mass and inertia of the patient’s hand are combined with those of the exoskeleton as a whole. The mass-inertial characteristics of the upper limb are selected according to (Tözerem, 2000) and are given in percentages with respect to the weight of the individual. For a human that weighs 70 kg, the upper limb’s mass (arm, forearm, and hand) is  $M_h = 3.472$  kg, the coordinates of the mass center are  $\rho_h = [0.298; 0]^T$  m and the upper limb’s inertia to the axis of joint J2 is  $J_h = 0.533$  kg m<sup>2</sup>. The total mass of the load is  $M_l = M_e + M_h = 4.354$  kg, the mass center coordinates are  $\rho = [0.283; 0.008]^T$ , and the total inertia is  $J_l = J_e + J_h = 0.594$  kg m<sup>2</sup>.

The motor drives the load and then the efficiency function has the form  $C=1/\eta$ . The values of the other mechanical parameters from equations (11) and (12) are shown in Table 1. Harmonic movements are simulated using equations (6), (7), and (8) with an increasing frequency and an amplitude of  $q_m = 40^\circ$  over the initial position  $q_0 = 235^\circ$ . Figure: 8 shows the variation of the motor’s inertial torque (12), the total load’s inertial torque (13), the viscous and Coulomb friction torque (11) and the torque of the total gravity (10). Figure: 9 shows the sum of the torques (10), (11), (12), and (13) as the total resistance in the joint according to equation (9).

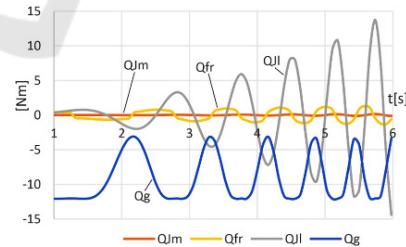


Figure 8: Torques from motor’s inertia  $Q_{Jm}$ , total load’s inertia  $Q_{Jl}$ , viscous and Coulomb friction  $Q_{fr}$ , and gravity of the total load  $Q_g$ , which are generated by the harmonic joint motion with a uniform increase in the frequency.

To overcome the resistive torque in the joint, the control algorithm creates a command for a desired torque to the pneumatic drive. It is set by determining the pressures  $p_a$  and  $p_b$  of the PAM actuators, according to (1), (2), and (3). Due to the slow force response of the PAM actuators, the pneumatic

actuation mainly performs the low-frequency part of the job. For this reason, in the simulation performed, the torque of pneumatic actuation is considered to be the result of constant supply pressures. Thus, Figure:9 shows the variation of the pneumatic drive torque  $Q_p$  for the pressures  $p_a = 300$  kPa and  $p_b = 0$ . At these pressures and at a set position, for example,  $q_0 = 235^\circ$ , the pneumatic drive acts as an elastic gravity load balancer. However, when the arm is diverted from this position, passive torque is generated due to the elastic deviation in the PAM actuators. In the simulations that were performed, the maximum value of the elastic deviations is set ( $q_m = 40^\circ$ ) for which the torque variations are evaluated. The resultant torque in the joint, according to (15) is shown in Fig.10. This is a command to the electric drive.

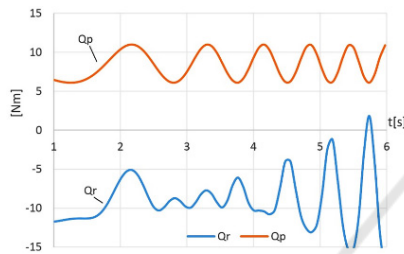


Figure 9: Total resistance in the joint  $Q_r$  as a sum of the torques  $Q_{jm}$ ,  $Q_{jl}$ ,  $Q_{fr}$  and  $Q_g$  as well the pneumatic drive torque  $Q_p$  at the PAM actuator pressures of  $p_a = 300$  and  $p_b = 0$  kPa.

It is seen from Figure:10 a) that the resulting joint torque (15) in its main part is compensated by the pneumatic drive. As a force command to the electric drive, the torque  $Q_e$  will complement the pneumatic drive. Figure: 10 b) shows the electric drive torque  $Q_m$  when it is calculated according to (16) with respect to the axis of the motor, taking into account the gearbox efficiency function  $C$  and the gear ratio  $n$ :

$$Q_m = Q_e \frac{C}{n} \tag{16}$$

The simulations show that with respect to the performance of the cyclical movements over the position  $q_0 = 235^\circ$  with an amplitude  $q_m = 40^\circ$  and a frequency up to 6 rad/s, the electric motor's torque  $Q_m$  does not exceed the motor nominal torque, as shown in Table 1. It also includes compensation for the elastic forces of parallel pneumatic drive. This is an extreme case since the actual pneumatic drive also performs the set force command so that the joint hybrid drive has the capacity to perform the desired joint torque.

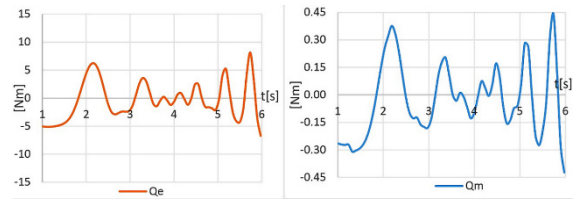


Figure 10: Resulting joint torque as a command: a) to the axis of the joint; b) to the axis of the motor.

## 5 DISCUSSION

In the simulations performed, the patient-initiated interaction torque is determined by passive forces, such as inertial, friction, and gravitational forces, and by the elasticity of the pneumatics (14). This is an extreme case of patient load. With active control (Figure: 3), the torque from the electric drive  $Q_e$  seeks to compensate for the torque in equation (14). However, safety and transparency are guaranteed by the low values of this torque that are obtained without feedback and active control. These values are a result of the passive approach in the design of a rehabilitation exoskeleton, which is built using lightweight parts, low geared motors, and compliant PAM actuators acting as gravity compensators.

The peak values of the resulting joint torques, as represented in Figure: 7 and Figure: 10, at low frequencies are mainly influenced by the gravity and the elasticity of the PAM actuators, while at high frequencies, they are mainly due to the inertial forces of the exoskeleton and the patient. For low-frequency rehabilitation tasks, the torque can be compensated by a feedforward control based only on the gravity models and the models of the elasticity of the pneumatic actuators. For high-frequency tasks, the compensation should include inertial models, and measuring or calculating the joints' acceleration.

The experiment shows that using the hybrid drive approach, the pneumatic drive relieves the electric drive by compensating mainly for the gravitational loads. The natural compliance of this drive, however, results in elastic forces that are compensated by the electric drive. When the pressure of the pneumatic actuators is low, such as in the "patient in charge" mode, the magnitude of the force command to the electric drive is not high. Increasing the pressure in the pair of pneumatic actuators, such as in the "robot in charge mode", increases the passive stiffness in the joint and hence increases the magnitude of the elastic force.

## 6 CONCLUSIONS

In this paper, an upper arm exoskeleton for rehabilitation and training is studied. An appropriate solution is sought for the exoskeleton design and actuation that provides transparency and natural safety on the one hand and force impact and performance on the other hand. A hybrid actuation approach is used, which consists of back drivable electric and pneumatic drives operating in parallel. In the paper, the feasibility of the basic therapy modes “patient in charge” and “robot in charge” is simulated. The approach for the dynamic estimation of elastic actuation through imposed motions is used. Harmonic motion with a uniform increase in the frequency in the second joint is simulated. In the “patient in charge” mode, the resistive torque of the passive impedance is seen as the interaction torque that is applied to the patient's hand. In the “robot in charge” mode, the resistive torque is used to assign force commands to the electric drive to perform feedforward compensations. Future exoskeleton experiments are planned in which the real parameters of the harmonic movements should be measured and evaluated.

## ACKNOWLEDGEMENTS

This research was supported by the National Science Fund, Project No. DN07/9 and by the Nat. Scientific Program ICTinSES, Contract No DO1–205.

## REFERENCES

- Jarrasse N, Proietti T, Crocher V, et al., 2014. Robotic Exoskeletons: A Perspective for the Rehabilitation of Arm Coordination in Stroke Patients. *Frontiers in Human Neuroscience*, Vol.8, Art.947: 1-13.
- Hogan N, Krebs HI, et al., 2006. Motions or muscles? Some behavioral factors underlying robotic assistance of motor recovery. *J. Rehabil. Res. Dev.*, 43: 605–618.
- Bergamasco M, Allotta B, Bosio L, et al., 1994. An Arm Exoskeleton System for Teleoperation and Virtual Environment Applications. *IEEE Int'l Conf. Robot. Automat.*; 2: 1449–1454.
- Carignan C.R. and Cleary K.R., 2000. Closed- Loop Force Control for Haptic Simulation of Virtual Environments. *Haptics-e*, February 23, Vol. 1, No. 2: 1-14.
- Veneman JF, Ekkelenkamp R, Kruidhof R, et al., 2006. A series elastic and bowden cable based actuation for use as torque actuator in exoskeleton-type robots. *The Int. Journal of Robotics Research*; 25(3): 261-281.
- Verstraten T, Beckerle P, Furnémont R, et al., 2016. Series and Parallel Elastic Actuation: Impact of natural dynamics on power and energy consumption. *Mechanism and Machine Theory*; 102: 232–246.
- Daerden Fr. and Lefeber D., 2002. Pneumatic Artificial Muscles: actuators for robotics and automation. *Europ. J. of Mech. and Environmental Engineering*; 47,1:1–11.
- Caldwell D., Tsagarakis N., 2007. “Soft” exoskeletons for upper and lower body rehabilitation- design, control and testing. *Int. J. of Humanoid Robot.*, 4(3): 549–573.
- Sardellitti I., Park J., Shin D., Khatib O., 2007. Air muscle controller design in the distributed macro-mini (DM2) actuation approach. *IEEE/RSJ Int. Conf. on Intellig. Rob. and Systems*, San Diego, CA : 1822–1827.
- Noda T., Teramae T., et al., 2014. Development of an upper limb exoskeleton powered via pneumatic electric hybrid actuators with Bowden cable, *IEEE/RSJ. Int. Conf. on Intellig. Rob. and Systems*, Chicago, IL: 3573 – 3578.
- Aguilar-Sierra H, Yu W, Salazar S., Lopez R., 2015. Design and control of hybrid actuation lower limb exoskeleton. *Adv. in Mech. Engineering*, 7(6): 1–13.
- Shin D., Yeh X., Khatib O., 2014. A new hybrid actuation scheme with artificial pneumatic muscles and a magnetic particle brake for safe human– robot collabor. *The Int. Journ. of Robics Research.*, 33(4): 507–518.
- Perry J., Rosen J. and Burns S., 2007. Upper-limb powered exoskeleton design. *IEEE/ASME Trans. on Mechatronics*; Vol.12, No. 4: 408–417.
- Abane, A., Guiatni, M. et al., 2016. Mechatronics Design, Modeling and Preliminary Control of a 5 DOF Upper Limb Active Exoskeleton, *13 th Int. Conf. on Inform. in Control, Autom. and Rob. (ICINCO 2016)*, 2: 398-405.
- Ermolov, I., Knyazkov, et al., 2016. The Dead Zone Determination for Exoskeleton Arm with Double Mode Control System. *13th Int. Conf. on Inform. in Control, Autom. and Rob. (ICINCO 2016)*, 2: 274-279.
- Garrec P., Friconneau J., Measson Y., Perrot Y., 2008. Able, an innovative transparent exoskeleton for the upper-limb, *IEEE/RSJ Int. Conference on Intelligent Robots and Systems (IROS 2008)*: 1483–1488
- Chakarov D., Veneva Iv., et al., 2017. Design and Control of a Force Reflecting Arm Exoskeleton for Virtual Reality Applications. *14th Int. Conf. on Inform. in Contr., Aut. and Rob., (ICINCO 2017)*, 2/102: 335-342.
- Chou P., Hannaford B., 1996. Measurement and Modeling of McKibben Pneumatic Artificial Muscles. *IEEE TRANS on Robotics and Automation*, Vol.12, No1: 1-22.
- Schiele A., Letier P. et al., 2006. Bowden cable actuator for force-feedback exoskeletons. *IEEE Int. Conf. on Intelligent Robots and Systems*: 3599-3604.
- Giberti H, Cinquemani S, and Legnani G., 2010. Effects of transmission mechanical characteristics on the choice of a motor-reducer. *Mechatronics*; 20(5): 604–610.
- Tözerem A., 2000. *Human Body Dynamics: Classical Mechanis and Human Movements*. Berlin Heidelberg: Springer-Verlag, p.316.